AFRL-RX-WP-TP-2012-0279

ACOUSTOELASTIC LAMB WAVE PROPAGATION IN BIAXIALLY STRESSED PLATES (PREPRINT)

Navneet Gandhi, Jennifer E. Michaels, and Sang Jun Lee
Georgia Tech Research Group.

MARCH 2012

Approved for public release; distribution unlimited.
See additional restrictions described on inside pages

STINFO COPY

AIR FORCE RESEARCH LABORATORY
MATERIALS AND MANUFACTURING DIRECTORATE
WRIGHT-PATTERSON AIR FORCE BASE, OH 45433-7750
AIR FORCE MATERIEL COMMAND
UNITED STATES AIR FORCE

REPORT DOCUMENTATION PAGE

Form Approved
OMB No. 0704-0188

The public reporting burden for this collection of information is estimated to average 1 hour per response, including the time for reviewing instructions, searching existing data sources, searching existing data sources, gathering and maintaining the data needed, and completing and reviewing the collection of information. Send comments regarding this burden estimate or any other aspect of this collection of information, including suggestions for reducing this burden, to Department of Defense, Washington Headquarters Services, Directorate for Information Operations and Reports (0704-0188), 1215 Jefferson Davis Highway, Suite 1204, Arlington, VA 22202-4302. Respondents should be aware that notwithstanding any other provision of law, no person shall be subject to any penalty for failing to comply with a collection of information if it does not display a currently valid OMB control number. **PLEASE DO NOT RETURN YOUR FORM TO THE ABOVE ADDRESS**.

1. REPORT DATE *(DD-MM-YY)*	2. REPORT TYPE	3. DATES COVERED *(From - To)*
March 2012	Journal Article	1 March 2012 – 1 March 2012

4. TITLE AND SUBTITLE
ACOUSTOELASTIC LAMB WAVE PROPAGATION IN BIAXIALLY STRESSED PLATES (PREPRINT)

5a. CONTRACT NUMBER
FA8650-09-C-5206

5b. GRANT NUMBER

5c. PROGRAM ELEMENT NUMBER
62102F

6. AUTHOR(S)
Navneet Gandhi, Jennifer E. Michaels, and Sang Jun Lee

5d. PROJECT NUMBER
4349

5e. TASK NUMBER
41

5f. WORK UNIT NUMBER
LP106300

7. PERFORMING ORGANIZATION NAME(S) AND ADDRESS(ES)
Georgia Tech Research Group
505 10th NW
Atlanta, GA 30332-0001

8. PERFORMING ORGANIZATION REPORT NUMBER

9. SPONSORING/MONITORING AGENCY NAME(S) AND ADDRESS(ES)
Air Force Research Laboratory
Materials and Manufacturing Directorate
Wright-Patterson Air Force Base, OH 45433-7750
Air Force Materiel Command
United States Air Force

10. SPONSORING/MONITORING AGENCY ACRONYM(S)
AFRL/RXLP

11. SPONSORING/MONITORING AGENCY REPORT NUMBER(S)
AFRL-RX-WP-TP-2012-0279

12. DISTRIBUTION/AVAILABILITY STATEMENT
Approved for public release; distribution unlimited.

13. SUPPLEMENTARY NOTES
The U.S. Government is joint author of this work and has the right to use, modify, reproduce, release, perform, display, or disclose the work. PA Case Number and clearance date: 88ABW-2012-0266, 17 Jan 2012. Preprint journal article to be submitted to Journal of Acoustical Society of America. This document contains color.

14. ABSTRACT
Acoustoelasticity, or the change in elastic wave speeds with stress, is a well-studied phenomenon for bulk waves. The effect of stress on Lamb waves is not as well understood, although it is clear that anisotropic stresses will produce anisotropy in the Lamb wave dispersion curves. Here the theory of acoustoelastic Lamb wave propagation is developed for isotropic media subjected to a biaxial, homogeneous stress field. It is shown that, as expected, dispersion curves change anisotropically for most stresses, modes and frequencies. Interestingly, for some modefrequency combinations, changes in phase velocity dispersion curves are isotropic even for a biaxial stress field. Theoretical predictions are compared to experimental results for several Lamb wave modes and frequencies for uniaxial loads applied to an aluminum plate, and the agreement is reasonably good.

15. SUBJECT TERMS
Acoustoelasticity, Lamb Waves, wave propagation, biaxial stress, isotropic plates, bulk waves, anisotropic

16. SECURITY CLASSIFICATION OF:			17. LIMITATION OF ABSTRACT:	NUMBER OF PAGES	19a. NAME OF RESPONSIBLE PERSON (Monitor)
a. REPORT	b. ABSTRACT	c. THIS PAGE			Charles Buynak
Unclassified	Unclassified	Unclassified	SAR	38	19b. TELEPHONE NUMBER *(Include Area Code)* N/A

Acoustoelastic Lamb wave propagation in biaxially stressed plates

Navneet Gandhi[(a)], Jennifer E. Michaels,[(b)] and Sang Jun Lee[(a)]

School of Electrical and Computer Engineering,
Georgia Institute of Technology, Atlanta, Georgia 30332-0250

Acoustoelasticity, or the change in elastic wave speeds with stress, is a well-studied phenomenon for bulk waves. The effect of stress on Lamb waves is not as well understood, although it is clear that anisotropic stresses will produce anisotropy in the Lamb wave dispersion curves. Here the theory of acoustoelastic Lamb wave propagation is developed for isotropic media subjected to a biaxial, homogeneous stress field. It is shown that, as expected, dispersion curves change anisotropically for most stresses, modes and frequencies. Interestingly, for some mode-frequency combinations, changes in phase velocity dispersion curves are isotropic even for a biaxial stress field. Theoretical predictions are compared to experimental results for several Lamb wave modes and frequencies for uniaxial loads applied to an aluminum plate, and the agreement is reasonably good.

PACS numbers: 43.25.Dc, 43.25.Zx, 43.35.Cg

[(a)] Currently with Acellent Technologies, Inc., Santa Clara, California
[(b)] Electronic mail: jennifer.michaels@ece.gatech.edu

(Running title: Acoustoelastic Lamb Waves)

Approved for public release; distribution unlimited

I. INTRODUCTION

Guided waves in plates, which are known as Lamb waves, are of considerable practical interest for both nondestructive evaluation and structural health monitoring because of their ability to propagate relatively long distances while still maintaining sensitivity to damage [1,2]. Because of the long propagation distances, particularly as compared to most bulk wave NDE methods, Lamb wave are particularly sensitive to changes in the propagation environment, such as temperature, stress and surface conditions [3,4,5]. Here we consider the effect of stress on Lamb waves propagating in homogeneous and initially isotropic plate subjected to a homogeneous biaxial stress field.

The theory to explain the dependence of wave speed on stress, or acoustoelasticity, was developed by Hughes and Kelly by applying the Murnaghan theory of finite deformation to propagation of bulk elastic waves in an initially isotropic solid subjected to a static predeformation [6]. They specifically consider the cases of hydrostatic pressure and uniaxial compressive stresses and derive expressions for changes in shear and longitudinal wave speeds as a function of applied stress for known material properties. Their work was extended to materials of arbitrary symmetry by Toupin and Bernstein [7]. One motivation of this early work in acoustoealasticity was measurement of third order elastic constants; however, this focus was largely shifted to measurement of both applied and residual stresses [8,9]. The comprehensive article in [10] provides a thorough treatment of acoustoelasticity with an emphasis on stress measurements via shear wave birefringence.

Acoustoelastic Rayleigh waves have also been quite thoroughly investigated, e.g., [11,12], but there are significantly fewer published works on acoustoelastic Lamb waves. Husson [13] considered acoustoelastic Lamb waves from a theoretical point of view and, among other things,

Approved for public release; distribution unlimited

predicted a strong frequency dependence of the acoustoelastic constants. Qu and Liu [14] generated dispersion curves for waves propagating in a stressed aluminum plate, but did not investigate dependence on the direction of propagation. Rizzo and Lanza di Scalea [15] measured changes in wave speed with tensile loads for guided waves in bars, and found a strong frequency dependence of the acoustoelastic constants. Lematre *et al.* [16] developed theory for Lamb wave propagation in stressed piezoelectric plate structures but showed only numerical results for propagation along the direction of the applied uniaxial load. An *in situ* structural health monitoring experiment by Michaels *et al.* [17] clearly show changes in wave speed as a function of direction of propagation, but no theory is presented. The semi-analytical finite element method has been applied to acoustoelastic wave propagation in bar-like structures (i.e., rails) [18].

In this paper the theory of acoustoelastic Lamb wave propagation in a homogeneous and initially isotropic plate is developed for an applied homogeneous biaxial stress by combining the theories of bulk wave acoustoelasticity and anisotropic guided wave propagation. The resulting analytical equations are solved numerically to show the anisotropic changes in dispersion for various applied stresses, and these changes are validated via experiments using an aluminum plate. Preliminary results of this present study have been previously reported by the authors [19,20].

II. REVIEW OF BULK WAVE ACOUSTOELASTICITY

The theory of bulk wave acoustoelasticity is reviewed here following the development of Pao and Gamer [21]. Referring to Figure 1, a body is deformed from its unstressed, or natural, state, to a statically deformed, or initial, state; the final state is that of wave motion superposed on the initial state. Coordinates ξ refer to a material point in the natural state, coordinates $\mathbf{X}$ refer to a

Approved for public release; distribution unlimited

material point in the initial state, and coordinates **x** to a material point in the final state. Deformations between the various states; i.e., natural to initial, natural to final, and initial to final, are given by $\mathbf{u}^{\mathrm{i}}$, $\mathbf{u}^{\mathrm{f}}$, and **u**, respectively:

$$\begin{aligned} \mathbf{u}^{\mathrm{i}}(\boldsymbol{\xi}) &= \mathbf{X} - \boldsymbol{\xi}, \\ \mathbf{u}^{\mathrm{f}}(\boldsymbol{\xi}, t) &= \mathbf{x} - \boldsymbol{\xi}, \\ \mathbf{u}(\boldsymbol{\xi}, t) &= \mathbf{x} - \mathbf{X} = \mathbf{u}^{\mathrm{f}}(\boldsymbol{\xi}, t) - \mathbf{u}^{\mathrm{i}}(\boldsymbol{\xi}). \end{aligned} \tag{1}$$

To describe wave propagation in a stressed medium, the equation for **u,** the incremental deformation between the initial and final states in a pre-stressed medium must be obtained.

Keeping the same convention as is used in [21], Greek subscripts indicate that the quantities are expressed in terms of the natural, or unstressed coordinates. Lagrangian strain tensors in the initial and final states are,

$$\begin{aligned} E^{\mathrm{i}}_{\alpha\beta} &= \frac{1}{2}\left(\frac{\partial u^{\mathrm{i}}_{\alpha}}{\partial \xi_{\beta}} + \frac{\partial u^{\mathrm{i}}_{\beta}}{\partial \xi_{\alpha}} + \frac{\partial u^{\mathrm{i}}_{\lambda}}{\partial \xi_{\alpha}} \frac{\partial u^{\mathrm{i}}_{\lambda}}{\partial \xi_{\beta}} \right), \\ E^{\mathrm{f}}_{\alpha\beta} &= \frac{1}{2}\left(\frac{\partial u^{\mathrm{f}}_{\alpha}}{\partial \xi_{\beta}} + \frac{\partial u^{\mathrm{f}}_{\beta}}{\partial \xi_{\alpha}} + \frac{\partial u^{\mathrm{f}}_{\lambda}}{\partial \xi_{\alpha}} \frac{\partial u^{\mathrm{f}}_{\lambda}}{\partial \xi_{\beta}} \right). \end{aligned} \tag{2}$$

Note that summation over repeated indices is implied here and in subsequent equations. If the wave motion is small compared to the initial predeformation, the incremental strain tensor between the initial and final states is given approximately by,

$$E_{\alpha\beta} = E^{\mathrm{f}}_{\alpha\beta} - E^{\mathrm{i}}_{\alpha\beta} = \frac{1}{2}\left(\frac{\partial u_{\alpha}}{\partial \xi_{\beta}} + \frac{\partial u_{\beta}}{\partial \xi_{\alpha}} + \frac{\partial u^{\mathrm{i}}_{\lambda}}{\partial \xi_{\alpha}} \frac{\partial u_{\lambda}}{\partial \xi_{\beta}} + \frac{\partial u^{\mathrm{i}}_{\lambda}}{\partial \xi_{\beta}} \frac{\partial u_{\lambda}}{\partial \xi_{\alpha}} \right). \tag{3}$$

If it is assumed that the material is hyperelastic, the Lagrangian strain tensor can be related to the second Piola-Kirchoff stress tensor via a constitutive equation; here only the second and third order elastic constants are retained:

Approved for public release; distribution unlimited

$$T^{\mathrm{i}}_{\alpha\beta} = C_{\alpha\beta\gamma\delta} E^{\mathrm{i}}_{\gamma\delta} + \tfrac{1}{2} C_{\alpha\beta\gamma\delta\varepsilon\eta} E^{\mathrm{i}}_{\gamma\delta} E^{\mathrm{i}}_{\varepsilon\eta},$$
$$T^{\mathrm{f}}_{\alpha\beta} = C_{\alpha\beta\gamma\delta} E^{\mathrm{f}}_{\gamma\delta} + \tfrac{1}{2} C_{\alpha\beta\gamma\delta\varepsilon\eta} E^{\mathrm{f}}_{\gamma\delta} E^{\mathrm{f}}_{\varepsilon\eta}. \tag{4}$$

Incremental stresses and strains between the initial and final states are related by subtracting the above equations and discarding higher order terms,

$$T_{\alpha\beta} = C_{\alpha\beta\gamma\delta} E_{\gamma\delta} + C_{\alpha\beta\gamma\delta\varepsilon\eta} e^{\mathrm{i}}_{\gamma\delta} e_{\varepsilon\eta}\,. \tag{5}$$

The infinitesimal initial and incremental strain tensors are,

$$e^{\mathrm{i}}_{\gamma\delta} = \frac{1}{2}\left(\frac{\partial u^{\mathrm{i}}_{\gamma}}{\partial \xi_{\delta}} + \frac{\partial u^{\mathrm{i}}_{\delta}}{\partial \xi_{\gamma}} \right), \quad e_{\varepsilon\eta} = \frac{1}{2}\left(\frac{\partial u_{\varepsilon}}{\partial \xi_{\eta}} + \frac{\partial u_{\eta}}{\partial \xi_{\varepsilon}} \right). \tag{6}$$

Equation (5) is thus the incremental constitutive equation.

Consider the equation of equilibrium for the static predeformation and the equation of motion for the final state,

$$\frac{\partial}{\partial \xi_{\beta}} \left[T^{\mathrm{i}}_{\beta\alpha} + T^{\mathrm{i}}_{\beta\gamma} \frac{\partial u^{\mathrm{i}}_{\alpha}}{\partial \xi_{\gamma}} \right] = 0, \quad \frac{\partial}{\partial \xi_{\beta}} \left[T^{\mathrm{f}}_{\beta\alpha} + T^{\mathrm{f}}_{\beta\gamma} \frac{\partial u^{\mathrm{f}}_{\alpha}}{\partial \xi_{\gamma}} \right] = \rho^{0} \frac{\partial^{2} u^{\mathrm{f}}_{\alpha}}{\partial t^{2}}, \tag{7}$$

where ρ^0 is the density in the natural state. The equation of motion for the incremental displacement is obtained by subtracting these two equations and neglecting one higher order term [21]. The resulting equation of motion for the incremental displacement is,

$$\frac{\partial}{\partial \xi_{\beta}} \left[T_{\alpha\beta} + T^{\mathrm{i}}_{\beta\gamma} \frac{\partial u_{\alpha}}{\partial \xi_{\gamma}} + T_{\beta\gamma} \frac{\partial u^{\mathrm{i}}_{\alpha}}{\partial \xi_{\gamma}} \right] = \rho^{0} \frac{\partial^{2} u_{\alpha}}{\partial t^{2}}\,. \tag{8}$$

Further simplification is possible by assuming that both the material and the static predeformation are homogeneous, and then substituting Eq. (5), the incremental constitutive equation, into Eq. (8). The resulting equation of motion for the incremental displacement is,

Approved for public release; distribution unlimited

$$A_{\alpha\beta\gamma\delta}\frac{\partial^2 u_\gamma}{\partial\xi_\beta\partial\xi_\delta}=\rho^0\frac{\partial^2 u_\alpha}{\partial t^2}, \tag{9}$$

where

$$A_{\alpha\beta\gamma\delta}=C_{\alpha\beta\gamma\delta}+C_{\beta\delta\varepsilon\eta}e^{\mathrm{i}}_{\varepsilon\eta}\delta_{\alpha\gamma}+C_{\alpha\beta\lambda\delta}\frac{\partial u^{\mathrm{i}}_\gamma}{\partial\xi_\lambda}+C_{\lambda\beta\gamma\delta}\frac{\partial u^{\mathrm{i}}_\alpha}{\partial\xi_\lambda}+C_{\alpha\beta\gamma\delta\varepsilon\eta}e^{\mathrm{i}}_{\varepsilon\eta}. \tag{10}$$

Equation (9) appears almost identical to the usual elastic wave equation, but it should be noted that **A** does not have the same symmetries as the stiffness tensor **C.** The only symmetry is $A_{ijkl} = A_{klij}$; in general, $A_{ijkl} \neq A_{jikl} \neq A_{ijlk}$.

III. THEORY OF LAMB WAVE ACOUSTOELASTICITY

Development of the theory to explain the propagation of Lamb waves in pre-stressed plates requires combining the equation of motion and constitutive equation developed for bulk waves in the previous section with the theory for Lamb wave propagation in an anisotropic plate. The equations derived in the process closely match those of Nayfeh and Chimenti [22] for anisotropic Lamb waves.

The geometry and coordinate system used in this paper are illustrated in Figure 2. Referring to the figure, the initial stresses are specified in the primed coordinate system, and a Lamb wave propagating along any arbitrary angle φ from the x_1' direction is considered. The unprimed coordinate system is rotated through the same angle φ to form the primed coordinate system, and analysis is performed in the unprimed system to simplify the mathematics. For an applied biaxial stress along the x_1' and x_2' directions, the initial stress tensor can be written as,

$$\mathbf{T}'=\begin{bmatrix}\sigma_{11} & 0 & 0\\ 0 & \sigma_{22} & 0\\ 0 & 0 & 0\end{bmatrix}. \tag{11}$$

Approved for public release; distribution unlimited

It is expressed in the unprimed system via a rotational transformation,

$$T_{ij}^{\mathrm{i}} = \beta_{im}\beta_{jn}T_{mn}^{\mathrm{i}}{}', \tag{12}$$

where β_{ij} is the cosine of the angle between the x_i and the x_j' axes. For convenience, in this and subsequent equations, lower case Roman subscripts are used instead of Greek subscripts to represent quantities in the natural coordinate system. In particular, all quantities are expressed in terms of the natural coordinates; for example, x_j is used instead of ξ_j.

Assuming that the initial strains are small, the constitutive equation relating initial stresses and strains given in Eq. (4) can be simplified to,

$$T_{ij}^{\mathrm{i}} = C_{ijkl}e_{kl}^{\mathrm{i}}. \tag{13}$$

For a given applied stress field, the strains in the unprimed system can be calculated by inverting this equation. From this point forward, all quantities are expressed in the unprimed system.

The **A** tensor as given by Eq. (10) can be simplified further by noting that the displacement derivatives can be expressed in terms of strains because for the stresses given in Eq. (11), the rotation terms are zero for all angles φ. Thus,

$$\frac{\partial u_j^{\mathrm{i}}}{\partial x_k} = e_{jk}^{\mathrm{i}}, \tag{14}$$

and

$$A_{ijkl} = C_{ijkl} + C_{jlmn}e_{mn}^{\mathrm{i}}\delta_{ik} + C_{ijml}e_{km}^{\mathrm{i}} + C_{mjkl}e_{im}^{\mathrm{i}} + C_{ijklmn}e_{mn}^{\mathrm{i}}. \tag{15}$$

The incremental stress-strain relation of Eq. (5) can similarly be simplified to

$$T_{ij} = B_{ijkl}\frac{\partial u_k}{\partial x_l}, \quad B_{ijkl} = C_{ijkl} + C_{ijml}e_{km}^{\mathrm{i}} + C_{ijklmn}e_{mn}^{\mathrm{i}}. \tag{16}$$

Approved for public release; distribution unlimited

Acoustoelastic Lamb wave propagation for a homogeneous and biaxial stress field requires solving the wave equation for the incremental displacements as given by Eq. (9) subject to stress-free boundary conditions at $x_3 = \pm d/2$ with the tensor **A** given by Eq. (15) and the stresses given by Eq. (16). This problem differs from Lamb wave propagation in anisotropic media in two regards: (1) as previously noted, the tensor **A** does not have the same symmetries as the stiffness tensor **C**, and (2) the boundary conditions at the plate surfaces are now written in terms of the incremental displacements.

Following [22], the approach to solving this problem is to assume solutions of the form,

$$u_j = U_j e^{i\xi(x_1 + \alpha x_3 - ct)}, \tag{17}$$

where ξ is the wavenumber in the x_1 direction, c is the phase velocity along the x_1 axis and α is the ratio of x_3 to x_1 wavenumbers. For a specific value of c, these solutions correspond to up-going and down-going bulk waves in the x_1–x_3 plane of the plate, which are then summed together to form the Lamb wave. This approach is sometimes referred to as the partial wave technique [23].

Substitution of Eq. (17) into Eq. (9) yields a form of the Christoffel equations,

$$K_{mn}(\alpha) U_n = 0, \tag{18}$$

where the parameters K_{mn} are given by,

$$\begin{aligned}
K_{11} &= c^2\rho^0 - A_{1111} - \alpha^2 A_{1313}, \\
K_{22} &= c^2\rho^0 - A_{1212} - \alpha^2 A_{2323}, \\
K_{33} &= c^2\rho^0 - A_{1313} - \alpha^2 A_{3333}, \\
K_{12} &= K_{21} = -A_{1112} - \alpha^2 A_{1323}, \\
K_{13} &= K_{31} = -\alpha(A_{1133} + A_{1331}), \\
K_{23} &= K_{32} = -\alpha(A_{1233} + A_{1332}).
\end{aligned} \tag{19}$$

Approved for public release; distribution unlimited

It can be seen that $K_{mn}=K_{nm}$. For existence of non-trivial solutions for the displacement amplitudes U_n, the determinant of the K matrix must go to zero, which produces a 6th order equation in α with six solutions α_q, q = 1…6. The coefficients of the odd powers of α are all zero, resulting in a cubic equation in α^2 given by

$$P_6\alpha^6 + P_4\alpha^4 + P_2\alpha^2 + P_0 = 0, \tag{20}$$

where the coefficients are listed in Appendix A. For a specific value of the Lamb wave phase velocity c, solving this cubic equation yields six values of α, which correspond to three up-going bulk waves and three down-going bulk waves.

The next step is to satisfy the stress-free boundary conditions on the plate surfaces as per Eq. (16). The approach taken here is similar to that taken in [22], and consists of constructing displacement ratios of U_2 and U_3 to U_1 for each of the six values of α,

$$V_q = \frac{U_{2q}}{U_{1q}}, \quad W_q = \frac{U_{3q}}{U_{1q}}, \quad q = 1,2\ldots 6\,. \tag{21}$$

Equation (18) enables each ratio to be expressed as a function of the K_{mn} and the corresponding α_q. The total displacement field of the Lamb wave is the sum of the displacements of the six partial waves,

$$\{u_1,u_2,u_3\} = \sum_{q=1}^{6}\left\{1,V_q,W_q\right\}U_{1q}e^{i\xi(x_1+\alpha_q x_3-ct)}. \tag{22}$$

Similarly, an expression for the stresses can be derived by substituting Eq. (22) into Eq. (16). The three stress components in the x_3 direction are then written as a sum of stresses due to the six individual bulk waves,

$$\{T_{33},T_{13},T_{23}\} = \sum_{q=1}^{6} i\xi\left\{D_{1q},D_{2q},D_{3q}\right\}U_{1q}e^{i\xi(x_1+\alpha_q x_3-ct)}\,, \tag{23}$$

Approved for public release; distribution unlimited

where the parameters D_{mq} are given by,

$$\begin{aligned} D_{1q} &= B_{3311} + B_{3312}V_q + \alpha_q B_{3333}W_q, \\ D_{2q} &= \alpha_q \left(B_{1313} + B_{1323}V_q \right) + B_{1331}W_q, \\ D_{3q} &= \alpha_q \left(B_{1323} + B_{2323}V_q \right) + B_{1332}W_q. \end{aligned} \tag{24}$$

Applying the stress-free boundary conditions at the surface of the plate requires setting T_{13}, T_{23} and T_{33} to zero at $x_3 = \pm d/2$, and yields six equations in terms of the six displacement amplitudes, U_{1q}, of the six partial waves, $q = 1,2\ldots6$. The determinant of coefficients must go to zero to obtain nontrivial solutions for these six displacement amplitudes. This determinant is,

$$\begin{vmatrix} D_{11}E_1 & D_{12}E_2 & D_{13}E_3 & D_{14}E_4 & D_{15}E_5 & D_{16}E_6 \\ D_{21}E_1 & D_{22}E_2 & D_{23}E_3 & D_{24}E_4 & D_{25}E_5 & D_{26}E_6 \\ D_{31}E_1 & D_{32}E_2 & D_{33}E_3 & D_{34}E_4 & D_{35}E_5 & D_{36}E_6 \\ D_{11}\tilde{E}_1 & D_{12}\tilde{E}_2 & D_{13}\tilde{E}_3 & D_{14}\tilde{E}_4 & D_{15}\tilde{E}_5 & D_{16}\tilde{E}_6 \\ D_{21}\tilde{E}_1 & D_{22}\tilde{E}_2 & D_{23}\tilde{E}_3 & D_{24}\tilde{E}_4 & D_{25}\tilde{E}_5 & D_{26}\tilde{E}_6 \\ D_{31}\tilde{E}_1 & D_{32}\tilde{E}_2 & D_{33}\tilde{E}_3 & D_{34}\tilde{E}_4 & D_{35}\tilde{E}_5 & D_{36}\tilde{E}_6 \end{vmatrix} = 0, \tag{25}$$

where $E_q = e^{i\xi\alpha_q d/2}$ and $\tilde{E}_q = e^{-i\xi\alpha_q d/2}$. After several number of row and column operations, Eq. (25) decouples into two equations,

$$f_s(\omega, c) = D_{11}G_1 \cot(\gamma\alpha_1) + D_{13}G_3 \cot(\gamma\alpha_3) + D_{15}G_5 \cot(\gamma\alpha_5) = 0, \tag{26}$$

$$f_a(\omega, c) = D_{11}G_1 \tan(\gamma\alpha_1) + D_{13}G_3 \tan(\gamma\alpha_3) + D_{15}G_5 \tan(\gamma\alpha_5) = 0. \tag{27}$$

The first equation corresponds to the symmetric modes and the second one corresponds to the antisymmetric modes. In both equations $\gamma = \xi d/2 = \omega d/(2c)$, where ω is the angular frequency. The parameters G_m are given as

$$G_1 = D_{23}D_{35} - D_{33}D_{25},\ G_3 = D_{31}D_{25} - D_{21}D_{35},\ G_5 = D_{21}D_{33} - D_{31}D_{23}. \tag{28}$$

Approved for public release; distribution unlimited

Solving Eqs. (26) and (27) yields the dispersion curves relating phase velocity and angular frequency for the symmetric and antisymmetric Lamb wave modes, respectively. It should be noted that solving these equations is not trivial; a brief description of the numerical method is given in Appendix B.

IV. SELECTED ANALYTICAL RESULTS

This section presents dispersion curves generated by solving Eqs. (26) and (27) numerically for specific materials. The first material considered is 6061-T6 aluminum, which was selected to match subsequent experiments. Material constants used are listed in Table 1, and the third order elastic constants were taken from [24]. It should be noted that although third order elastic constants are available in the literature for several aluminum alloys [24,25,26], their values are quite variable. It is not clear whether the variability is caused by differences in experimental methods or actual material variations. The second material considered was steel because of its widespread use. Unfortunately third order elastic constants for steel are not widely reported; the ones used here are summarized in Table 2 and are for Hecla 37 steel [26].

Figures 3(a) and 3(b) present the family of symmetric and antisymmetric dispersion curves for aluminum under a uniaxial stress of $\sigma_{11} = 100$ MPa and for waves propagating at an angle of 45° to the stress direction; note that the SH_0 mode is not shown. To illustrate the variation of the function values as they go to zero, $\log|f_s(\omega,c)|$ and $\log|f_a(\omega,c)|$ have been plotted in the background for both plots. These dispersion curves appear virtually identical to the ones obtained using the Rayleigh-Lamb equations for the no-load case since the velocity changes due to the applied stress are not noticeable at this scale. These and all subsequent curves refer to phase velocities computed in the natural, or undeformed, coordinate system, which is consistent with the derivations of Section III.

Approved for public release; distribution unlimited

Figure 4 presents the variation of phase velocity of the S_0 mode at 250 kHz with angle for a range of biaxial stresses and for a plate thickness of 6.35 mm. Note that the load is applied along the *y* axis so that waves propagating along the direction of applied load are at 90°. An interesting prediction made by this plot is that the angle at which the phase velocity change is zero (about 27°) is independent of stress. It can also be seen that at a specific angle, the change of phase velocity is linear with load.

Figure 5 compares phase velocity changes as a function of frequency for the S_0 mode at varying unixial stresses σ_{11} for waves propagating at an angle of 45°. This plot shows large changes in phase velocity for lower frequencies that reduce and flatten in the high frequency region. It is evident that the change of phase velocity is linear with load at a specific frequency.

Figures 6(a) through 6(d) compare the phase velocity change with frequency at different angles for the S_0, S_1, A_0 and A_1 Lamb wave modes, respectively. The plot for A_0 is particular interesting in that it predicts isotropic phase velocities for the A_0 mode for the frequency-thickness product of approximately 187 MHz-mm, although at this frequency the velocity change from the unstressed condition is non-zero. This phenomenon should not be confused as isotropic wave propagation since the group velocity at this frequency is certainly angle dependent.

Figure 7 is a plot of the S_0 and SH_0 modes under the influence of applied uniaxial stress and shows interesting behavior. The S_0 and SH_0 modes split and form two new continuous modes at their original point of intersection (from the unstressed case) when a stress is applied. Because of symmetry, this splitting does not occur at either 0° or 90°, and is similar to that which also occurs for anisotropic materials [27,28]. In the earlier plots, this splitting was not shown to facilitate comparison of the perturbed mode to the S_0 mode of the unstressed material.

Approved for public release; distribution unlimited

Figure 8 shows the A_0 mode for steel under a uniaxial stress of $\sigma_{11} = 200$ MPa. Steel also shows the isotropic phase velocities at lower frequencies for the A_0 mode at a frequency-thickness product of approximately 0.35 MHz-mm. Additional results for steel are not shown because they are qualitatively the same as for aluminum.

V. EXPERIMENTAL RESULTS

An experiment was performed to measure changes in phase velocity as a function of applied load for various Lamb modes propagating in an aluminum plate with dimensions of 305 mm × 610 mm × 6.35 mm. The plate was instrumented with ten PZT discs as shown in Figure 9, and the transmitting transducers were excited by a five-cycle Hanning windowed sinusoid. The following three frequencies were utilized to produce an unambiguous first arrival of the indicated Lamb wave mode: 250 kHz (S_0 mode), 400 kHz (A_1 mode), and 600 kHz (S_1 mode). Signals were recorded from 9 of the 45 possible transmit-receive pairs as shown in Figure 9(b) at eleven uniaxial loads (0 MPa to 57.5 MPa in steps of 5.75 MPa).

Time shifts were measured by identifying a zero crossing in the center of each direct arrival echoes, and then tracking that zero crossing as a function of applied uniaxial load. For a particular time shift, the corresponding change in phase velocity can be calculated as [19],

$$\Delta c_p = -\frac{c_p^2 \Delta t}{d} . \tag{29}$$

Although there is also a change of distance, it does not appear in Eq. (28) because all computations are in the natural, or undeformed, coordinate system.

Figure 10(a) shows the linear variation of the changes in phase velocity with stress for propagation of the three Lamb wave modes along the direction of applied stress (the *y* axis). The results are further corroborated by experimental measurements using transducer #1 as a

Approved for public release; distribution unlimited

transmitter and transducer #6 as a receiver, which show similar linear changes in phase velocity. Figure 10(b) shows the variation of phase velocity with angle for the case of uniaxial stress of $\sigma_{22} = 57.5$ MPa. The experimental values were obtained by fitting a line to the time shift versus load curve, and then calculating the time shift at 57.5 MPa from the linear fit. Both theoretical and experimental data closely follow a sinusoidal profile. The systematic differences between theory and experiment are probably due to the well-known difficulties in accurately obtaining third order elastic constants. The linear dependence of phase velocity changes with load and sinusoidal dependence with angle of propagation is expected since that is the case for bulk waves, but it is reassuring that both characteristics are validated by both numerical and experimental results.

Figure 11, which us analogous to Figure 12(b), shows the variation of phase velocity with angle but with the theoretical curves calculated using different (but plausible) values for the TOECs. For these values, selected as l = -181 MPa, m = -289 MPa, and n = -336 MPa, the S_0 and A_1 theoretical curves are in excellent agreement with the experimental data, and the S_1 curve is in reasonable agreement. This significant improvement not only supports the speculation that the deviation between theory and experiment is largely explained by errors in TOECs, it also suggests that guided wave measurements could be used to estimate TOECs.

VI. SUMMARY AND CONCLUSIONS

Described here is the theory for acoustoelastic Lamb wave propagation, and both numerical and experimental results are shown for the multiple Lamb wave modes. Unlike bulk waves, the acoustoelastic behavior is frequency dependent. Experimental results that measure changes in phase velocity as a function of both load and propagation angle agree reasonably well with theory. Both numerical and experimental data show the expected linear dependence of phase

Approved for public release; distribution unlimited

velocity changes with load and sinusoidal dependence with angle of propagation, all at a single frequency. However, systematic differences between theory and experiment clearly indicate that additional measurements should be performed to independently measure third order elastic constants for the specific material under consideration.

The robustness of the Lamb wave results as a function of propagation angle suggest that Lamb wave measurements may provide an alternative means of measuring third order elastic constants. This would be challenging because unlike bulk wave measurements, there is no analytical expression relating third order elastic constants to measured time shifts, much less a closed form solution for the inverse problem. Thus, any means of using Lamb wave data to obtain third order elastic constants would have to be numerical in nature with the resulting issues of existence and uniqueness.

Additional experiments are also needed to verify some of the interesting theoretical predictions, particularly those shown in Figure 4(c) regarding isotropic phase velocities changes in the low frequency region for the A_0 mode. Future theoretical work should consider extension of this theory to materials of higher symmetry, which is believed to be straightforward but tedious. In terms of numerical work, there are certain regions in the anti-symmetric spectrum that may indicate the presence of roots (SH_0 like solutions), although they do not correspond to any mode for the unstressed case. Most likely these are false roots are caused by imperfections in the numerical method, but they need further investigation.

ACKNOWLEDGEMENTS

The authors gratefully acknowledge the support of the Air Force Research Laboratory, Contract No. FA8650-09-C-5206 (Charles Buynak, Program Manager).

Approved for public release; distribution unlimited

APPENDIX A. Polynomial Coefficients

Coefficients of the 6*th* order polynomial in Eq. (20) are as follows:

$$
\begin{aligned}
P_6 &= (A_{1323}^2 - A_{1313}A_{2323})A_{3333} \\
P_4 &= A_{1233}^2 A_{1313} + A_{1313}A_{1323}^2 - 2A_{1133}A_{1323}A_{1332} - 2A_{1323}A_{1331}A_{1332} + A_{1313}A_{1332}^2 \\
&\quad + 2A_{1233}(-A_{1323}(A_{1133} + A_{1331}) + A_{1313}A_{1332}) + A_{1133}^2 A_{2323} - A_{1313}^2 A_{2323} \\
&\quad + 2A_{1133}A_{1331}A_{2323} + A_{1331}^2 A_{2323} - (A_{1212}A_{1313} - 2A_{1112}A_{1323} + A_{1111}A_{2323})A_{3333} \\
&\quad + c^2\rho_0(-A_{1323}^2 + A_{1313}A_{2323} + (A_{1313} + A_{2323})A_{3333}) \\
P_2 &= A_{1133}^2 A_{1212} + A_{1111}A_{1233}^2 - A_{1212}A_{1313}^2 + 2A_{1112}A_{1313}A_{1323} - 2A_{1112}A_{1233}A_{1331} \\
&\quad + A_{1212}A_{1331}^2 + 2A_{1111}A_{1233}A_{1332} - 2A_{1112}A_{1331}A_{1332} + A_{1111}A_{1332}^2 \\
&\quad - 2A_{1133}(-A_{1212}A_{1331} + A_{1112}(A_{1233} + A_{1332})) - A_{1111}A_{1313}A_{2323} \\
&\quad + (A_{1112}^2 - A_{1111}A_{1212})A_{3333} - c^4\rho_0^2(A_{1313} + A_{2323} + A_{3333}) \\
&\quad + c^2\rho_0(-2A_{1112}A_{1323} - (A_{1133} + A_{1331})^2 - (A_{1233} + A_{1332})^2 \\
&\quad + A_{1313}(A_{1212} + A_{1313} + A_{2323}) + A_{1212}A_{3333} + A_{1111}(A_{2323} + A_{3333})) \\
P_0 &= (-A_{1112}^2 + (c^2\rho_0 - A_{1111})(c^2\rho_0 - A_{1212}))(c^2\rho_0 - A_{1313})
\end{aligned}
\tag{A1}
$$

Appendix B. Numerical Method

This appendix summarizes the steps of the numerical method for solving Eqs. (26) and (27) for the symmetric and antisymmetric modes.

The first step is to pick a plate wave velocity c and find the corresponding α_q from the polynomial in Eq. (20). Next, express Eq. (25) as

$$
\begin{aligned}
f_s(\omega, c) &= D_{11}G_1(\alpha_3, \alpha_5)\cot(\gamma\alpha_1) + D_{13}G_3(\alpha_1, \alpha_5)\cot(\gamma\alpha_3) + D_{15}G_5(\alpha_1, \alpha_3)\cot(\gamma\alpha_5) \\
&= D_{11}H_1(\alpha_1, \alpha_3, \alpha_5) + D_{13}H_3(\alpha_1, \alpha_3, \alpha_5) + D_{15}H_5(\alpha_1, \alpha_3, \alpha_5) = 0.
\end{aligned}
\tag{B1}
$$

For real α_q, all Ds, Gs and cotangent functions are real and therefore f_s is real. D_{1q} is even in α_q, D_{2q} and D_{3q} are odd in α_q, which implies $G_n(\alpha_p, \alpha_q)$ is odd in both α_p and α_q. Since $\cot(\gamma\alpha_q)$ is odd in α_q, $H_n(\alpha_p, \alpha_q, \alpha_r)$ is odd in all three α. For odd functions, the Taylor series has only odd

Approved for public release; distribution unlimited

terms and this implies that for imaginary arguments, the value of the odd functions is always imaginary. By carefully analyzing the symmetries for all terms it can be seen that for a mixture of real and imaginary αs, f_s has a value that is purely imaginary or purely real.

Next, based on the values of α, we pick one of two root finding algorithms:

(1) For values of c that produce purely imaginary and real values of α:

- Sweep across ω and find pairs of ω values where the value of f_s changes sign (this is not a problem since f_s values at all ω for this value of c are real or all imaginary). Each of the pairs thus obtained mark intervals in which solutions to the equation $f_s = 0$ are guaranteed to exist (and these intervals can be arbitrary small). These (ω, c) pairs constitute points on the dispersion curves.
- Any real value of α will produce infinities in the cotangent functions. Since a sign change occurs at aninfinity, these are actually false roots that must be handled by excluding pairs of ω values that correspond to multiples of $n\pi$ in the cotangent functions. Cotangents with imaginary values of α do not produce any infinities.

(2) For values of c with any complex values of α:

- Ds and Gs are complex valued and therefore f_s is complex valued. Sweep across ω for pairs of ω where both the real and imaginary components of f_s switch sign together. Also project real and imaginary components of the function value f_s on the $\theta = 45°$ and $\theta = 135°$ lines and check for sign changes in both projected directions. This procedure finds roots that occur when the curve of f_s as a function of ω is tangential to either the real or imaginary axis. Either a sign change in both real and imaginary components or ones in both projected values yields an interval with a solution. In general for this case, it is

Approved for public release; distribution unlimited

possible to get false solutions but these can be discarded later. Cotangents corresponding to complex values of α do not produce any infinities.

Finally, points that are nearby in the set of solutions are connected to obtain dispersion curves. Ambiguous regions can be scanned with higher resolutions to obtain more points. The exact same method applies to the function for antisymmetric modes f_a**.**

REFERENCES

1. J. L. Rose, "Guided wave nuances for ultrasonic nondestructive evaluation," *IEEE Trans. Ultrason, Ferroelect. Freq. Contr.*, **47**(3), pp. 575-583, 2000.

2. R. P. Dalton, P. Cawley, and M. J. S. Lowe, "The potential of guided waves for monitoring large areas of metallic aircraft fuselage structure," *Journal of Nondestructive Evaluation*, **20**(1), pp. 29-46, 2001.

3. A. J. Croxford, J. Moll, P. D. Wilcox, and J. E. Michaels, "Efficient temperature compensation strategies for guided wave structural health monitoring," *Ultrasonics*, **50**, pp. 517-528, 2010.

4. J. E. Michaels, S. J. Lee, and T. E. Michaels, "Effects of applied loads and temperature variations on ultrasonic guided waves," *Proc. 2010 European Workshop on Structural Health Monitoring*, DEStech Publications, Inc., Lancaster, PA, pp. 1267-1272, 2010.

5. Y. Lu and J. E. Michaels, "Feature extraction and sensor fusion for ultrasonic structural health monitoring under changing environmental conditions," *IEEE Sensors Journal*, **9**(11), pp. 1462-1471, 2009.

Approved for public release; distribution unlimited

6. D. S. Hughes and J. L. Kelly, “Second-order elastic deformation of solids,” *Phys. Rev.*, **92**, pp. 1145-1149, 1953.

7. R. A. Toupin and B. Bernstein, “Sound waves in deformed perfectly elastic materials. Acoustoelastic effect,” *J. Acoust. Soc. Am.*, **33**, pp. 216-225, 1961.

8. R. B. King and C. M. Fortunko, “Determination of in-plane residual stress states in plates using horizontally polarized shear waves,” *J. Appl. Phys.*, **54**(6), pp. 3027-3035, 1983..

9. R. B. Thompson, S. S. Lee, and J. F. Smith, “Angular dependence of ultrasonic wave propagation in a stressed orthorhombic continuum: Theory and application to the measurement of stress and texture,” *J. Acoust. Soc. Am.*, **80**(3), pp. 921-931, 1986.

10. Y.-H. Pao, W. Sachse, and H. Fukuoka, "Acoustoelasticity and ultrasonic measurement of residual stress," in *Physical Acoustics Volume XVII*, Eds. W. P. Mason and R. N. Thurston (Academic Press, New York), pp. 61-143, 1084.

11. M. Duquennoy, M. Ouaftouh, M. Ourak, and F. Jenot, “Theoretical determination of Rayleigh wave acoustoelastic coefficients: comparison with experimental values,” *Ultrasonics*, **39**, pp. 575-583, 2002.

12. Y. Iwashimizu and O. Kobori, “Rayleigh wave in a finitely deformed isotropic elastic material,” *J. Acoust. Soc. Am.*, **64**(3), pp. 910-916, 1978.

13. D. Husson, “A perturbation theory for the acoustoelastic effect of surface waves,” *J. Appl. Phys.*, **57**(5), pp. 1562-1568, 1985.

Approved for public release; distribution unlimited

14. J. Qu and G. Liu, “Effects of residual stress on guided waves in layered media,” *Rev. Prog. Quant. NDE,* **17**, D. O. Thompson and D. E. Chimenti (Eds.), Plenum Press, pp. 1635-1642, 1998.

15. P. Rizzo and F. Lanza di Scalea, “Effect of frequency on the acoustoelastic response of steel bars,” *Exp. Tech.*, **27**(6), pp. 40-43, 2003.

16. M. Lematre, G. Feuillard, T. Delaunay, and M. Lethiecq, “Modeling of ultrasonic wave propagation in integrated piezoelectric structures under residual stress,” *IEEE Trans. Ultrason. Ferroelect. Freq. Contr.*, **53**(4), pp. 685-696, 2006.

17. J. E. Michaels, T. E. Michaels and R. Martin, “Analysis of global ultrasonic sensor data from a full scale wing panel test,” *Rev. Prog. Quant. NDE*, **28A**, D. O. Thompson and D. E. Chimenti (Eds.), American Institute of Physics, pp. 950-957, 2009.

18. F. Chen and P. D. Wilcox, “The effect of load on guided wave propagation,” *Ultrasonics*, **47**, pp.111-122, 2007.

19. J. E. Michaels, N. Gandhi and S. J. Lee, “Acoustoelastic Lamb Waves and Implications for Structural Health Monitoring,” in *From Waves in Complex Systems to Dynamics of Generalized Continua – Tributes to Professor Yih-Hsing Pao on his 80th Birthday*, K. Hutter, T.-T. Wu and Y.-C. Shu (Eds.), World Scientific, Hackensack, New Jersey, Chapter 4, 2011.

20. N. Gandhi J. E. Michaels and S. J. Lee, "Acoustoelastic Lamb wave propagation in a homogeneous, isotropic aluminum plate," *Rev. Prog. Quant. NDE*, **30A**, D. O. Thompson and D. E. Chimenti (Eds.), American Institute of Physics, pp. 161-168, 2011.

Approved for public release; distribution unlimited

21. Y.-H. Pao and U. Gamer, "Acoustoelastic waves in orthotropic media," *J. Acoust. Soc. Am.*, **77**, pp. 806-812, 1985.

22. A. H. Nayfeh and D. E. Chimenti, "Free wave propagation in plates of general anisotropic media," *J. Appl. Mech.*, **56**, pp. 881-886, 1989.

23. J. L. Rose, *Ultrasonic Waves in Solid Media* (Cambridge University Press, 1999).

24. J. R. Asay and A.H. Guenther, "Ultrasonic studies of 1060 and 6061-T6 aluminum", *Journal of Applied Physics*, **38**, pp. 4086-4088, 1967.

25. M. Dubuget, R. El Guerjouma, S. Dubois, J. C. Baboux, and A. Vincent, "Characterization of the non-linear elastic properties of aluminium alloys using ultrasonic evaluation under load," *Materials Science Forum*, **217-222**, pp. 951-956, 1996.

26. R. T. Smith, R. Stern, and R. W. B. Stephens, "Third-order elastic moduli of polycrystalline metals from ultrasonic velocity measurements", *J. Acoust. Soc. Am.*, **40**, pp. 1002-1008, 1966.

27. Y. Li and R. B. Thompson, "Influence of anisotropy on the dispersion characteristics of guided ultrasonic plate modes," *J. Acoust. Soc. Am.*, **87**, pp. 1911-1931, 1990.

28. M. Castaings and B. Hosten, "Lamb and SH waves generated and detected by air-coupled ultrasonic transducers in composite material plates," *NDT&E International*, **34**, pp. 249-258, 2001.

Approved for public release; distribution unlimited

Table 1. Material constants for 6061-T6 aluminum [24].

Parameter	Value	Units
λ	54.308	GPa
μ	27.174	GPa
l	-281.5	GPa
m	-339.0	GPa
n	-416.0	GPa
ρ_0	2704	kg/m^3

Table 2. Material constants for Hecla 37 steel [26].

Parameter	Value	Units
λ	111	GPa
μ	821	GPa
l	-461	GPa
m	-636	GPa
n	-708	GPa
ρ_0	7823	kg/m^3

Approved for public release; distribution unlimited

LIST OF FIGURES

Approved for public release; distribution unlimited

Figure 8. (color online) Changes in phase velocity for the A_0 mode propagating in steel for a uniaxial load of 100 MPa applied along the *x* axis (0°). The inset plot shows that the changes are isotropic for a frequency-thickness product of approximately 0.35 MHz-mm.

Figure 9. (a) Photograph and (b) sketch of transducers mounted to a 6.35 mm thick aluminum plate. The sketch shows the nine propagation paths used to characterize acoustoelastic Lamb wave propagation.

Figure 10. (color online) Comparison of theory and experiment for propagation in aluminum (thickness of 6.35 mm) with an applied uniaxial load at 90°. (a) Changes in phase velocity versus load for waves propagating at an angle of 90°, and (b) changes in phase velocity versus propagation angle for an applied load of 57.5 MPa.

Figure 11. (color online) Comparison of theory and experiment with an applied uniaxial load of 57.5 GPa at 90° using modified TOECs (l = -181 MPa, m = -289 MPa, and n = -336 MPa).

Approved for public release; distribution unlimited

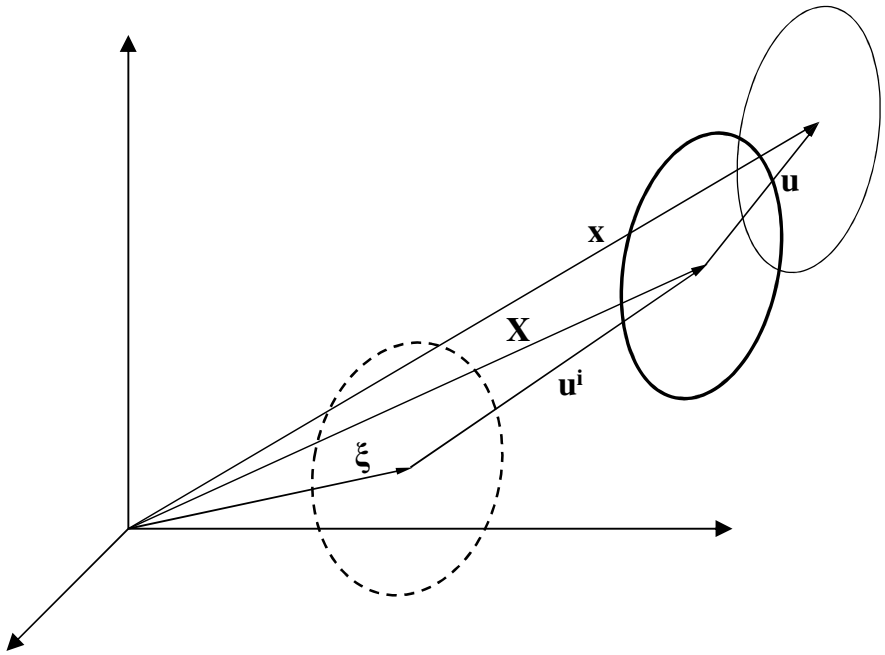

Figure 1. Deformation of a body from its natural (undeformed) state ξ to an initial state of static deformation **X** to a final state of wave motion **x**.

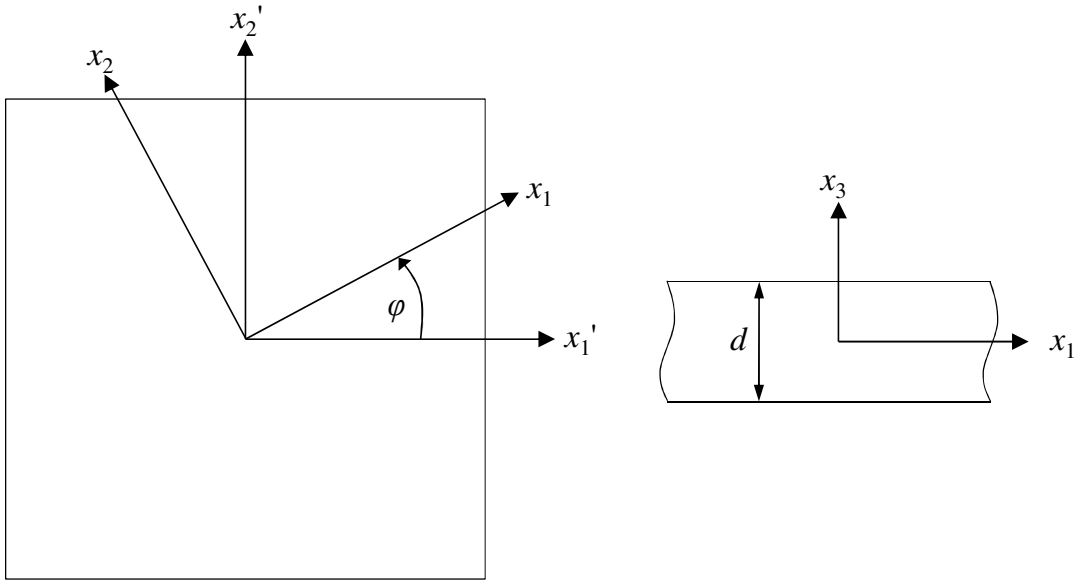

Figure 2. Geometry for Lamb wave propagation in a pre-stressed plate. Stresses are applied along the principal directions in the primed coordinate system, and Lamb waves propagate along the x_1 axis.

Approved for public release; distribution unlimited

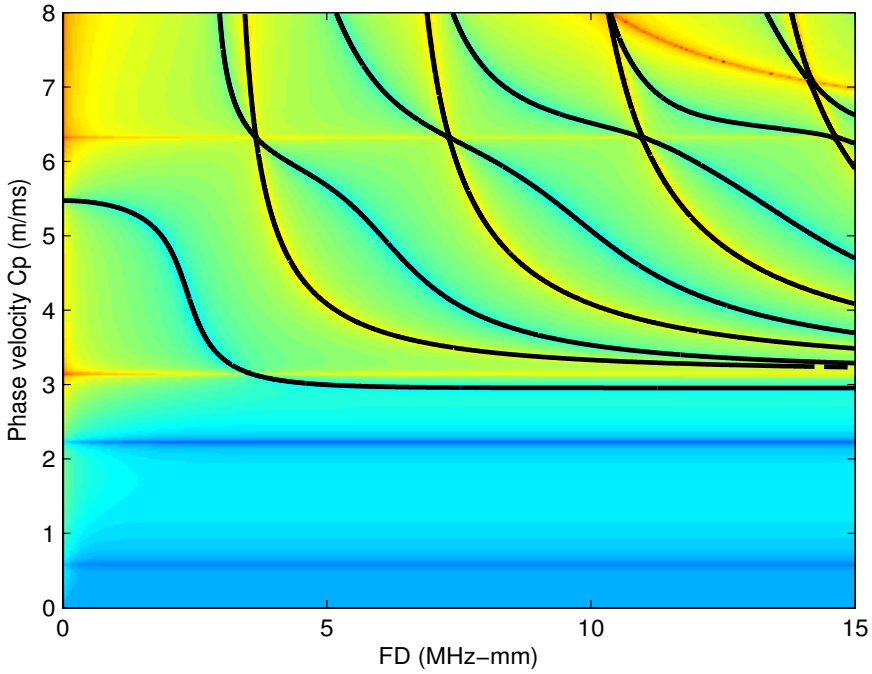

(a)

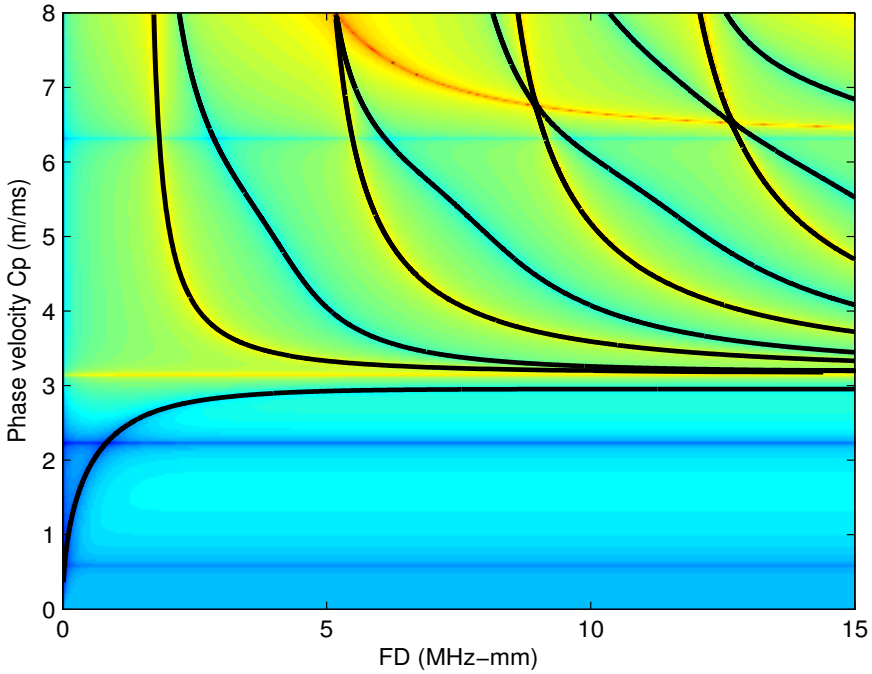

(b)

Figure 3. (color online) Dispersion curves for waves propagating in aluminum at an angle of 45° to an applied uniaxial applied stress of 100 MPa. (a) Symmetric modes, and (b) anti-symmetric modes.

Approved for public release; distribution unlimited

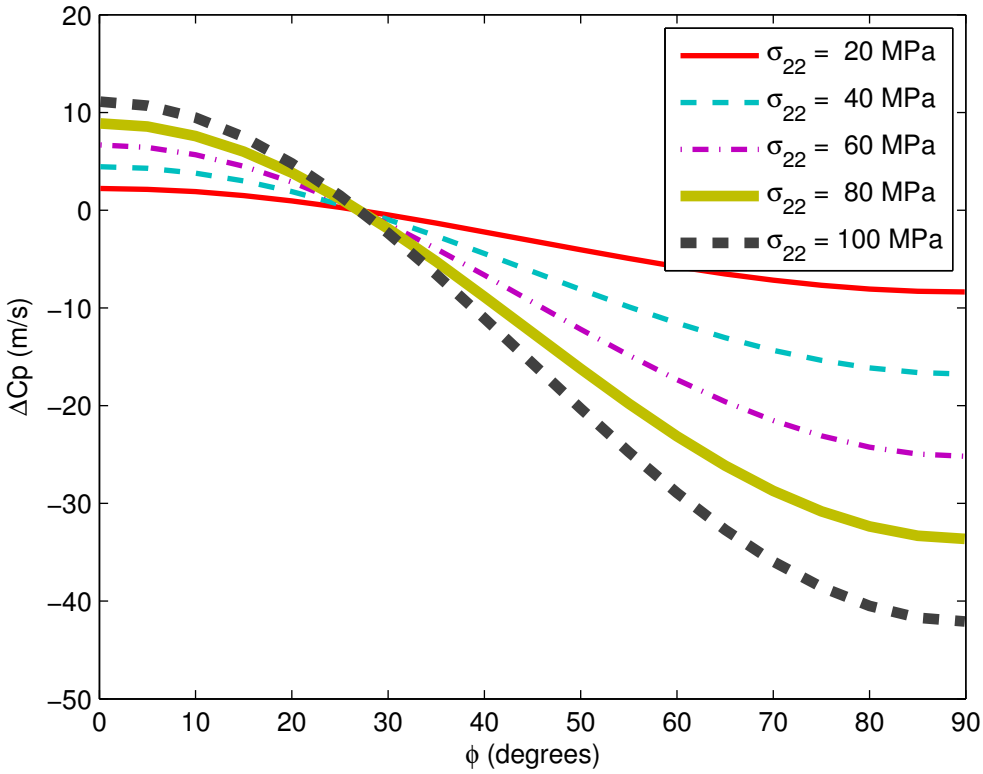

Figure 4. (color online) Change in phase velocity versus propagation angle for the S_0 mode in aluminum (thickness of 6.35 mm) at 250 kHz and for different uniaxial loads applied along the *y* axis (90°).

Approved for public release; distribution unlimited

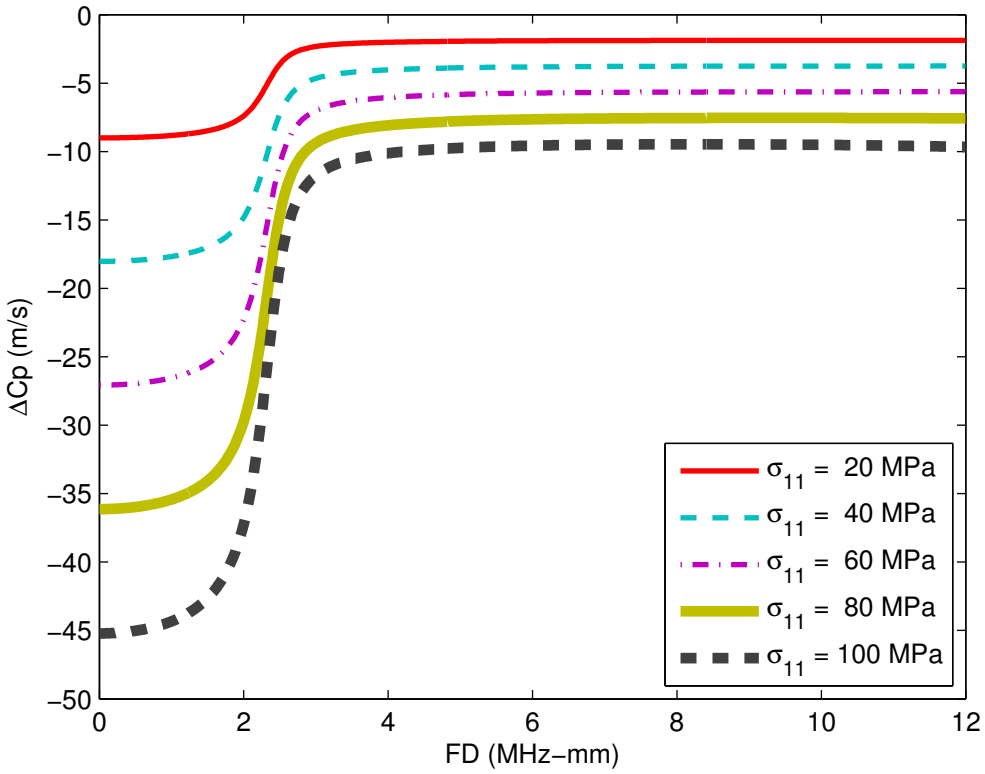

Figure 5. (color online) Change in phase velocity versus frequency for the S_0 mode propagating in aluminum at an angle of 45° to various uniaxial loads applied along the *x* axis.

Approved for public release; distribution unlimited

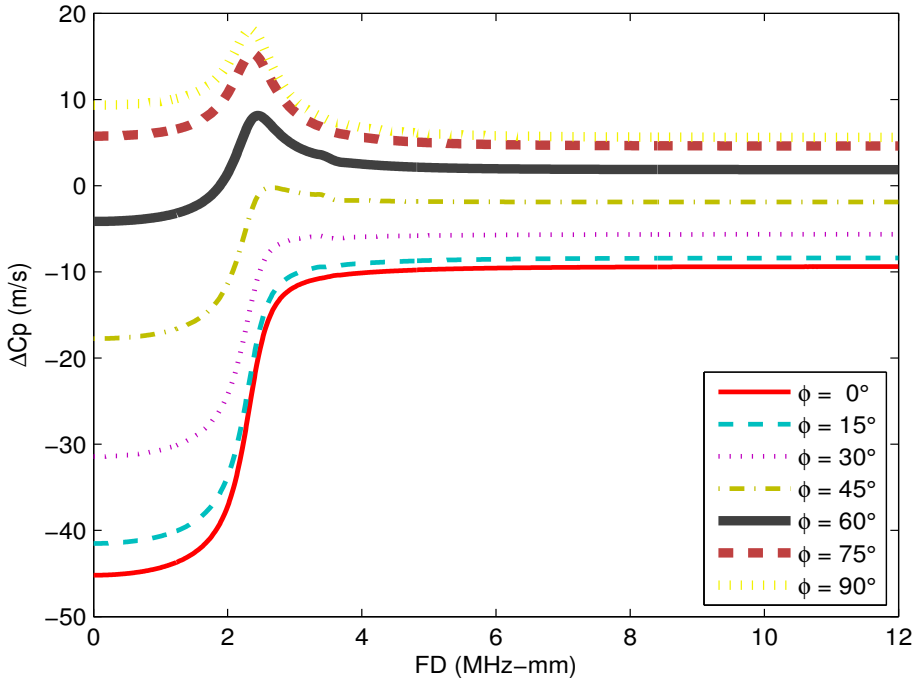

(a)

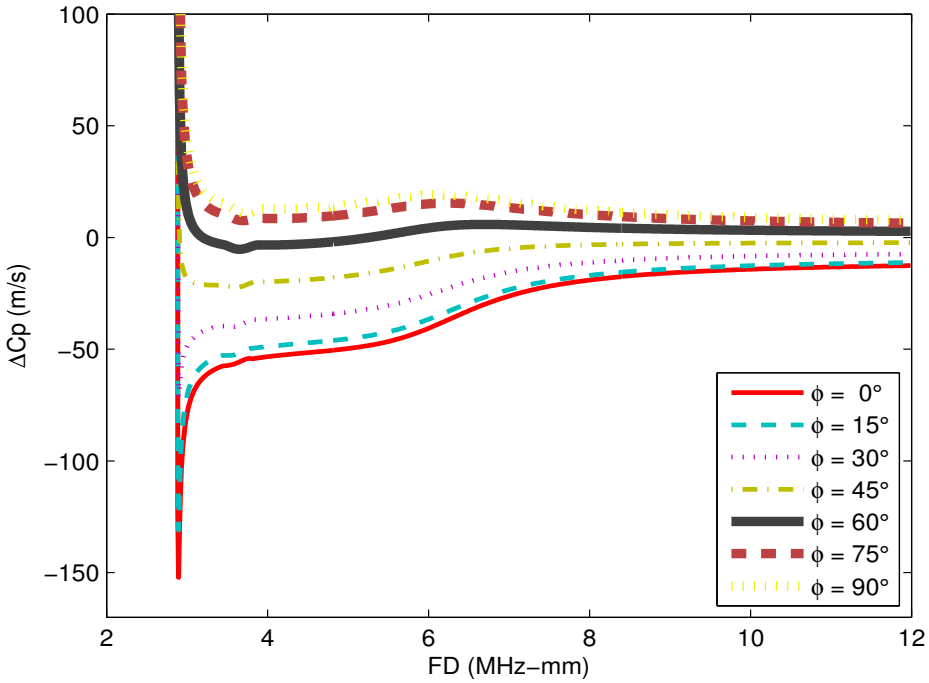

(b)

Approved for public release; distribution unlimited

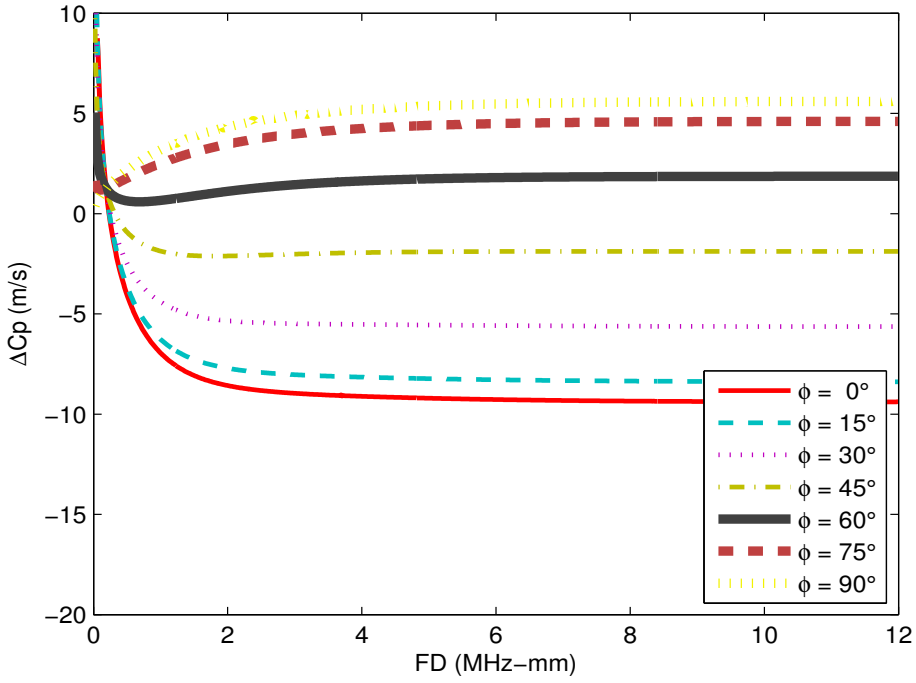

(c)

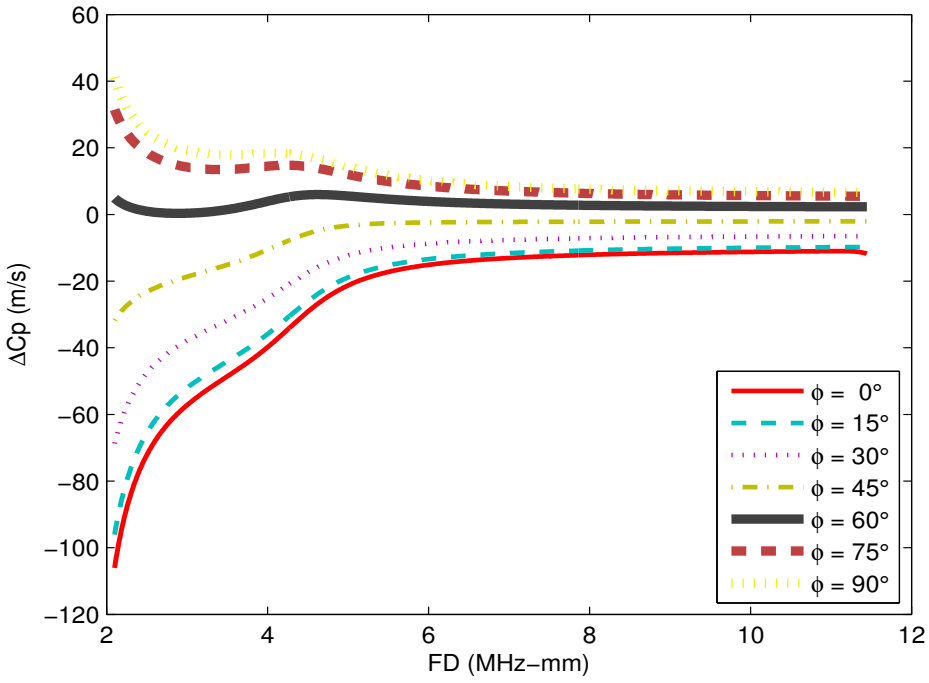

(d)

Figure 6. (color online) Changes in phase velocity versus frequency for waves propagation in aluminum at various angles to a 100 MPa uniaxial load applied at 0°. (a) S_0, (b) S_1, (c) A_0, and (d) A_1 mode.

Approved for public release; distribution unlimited

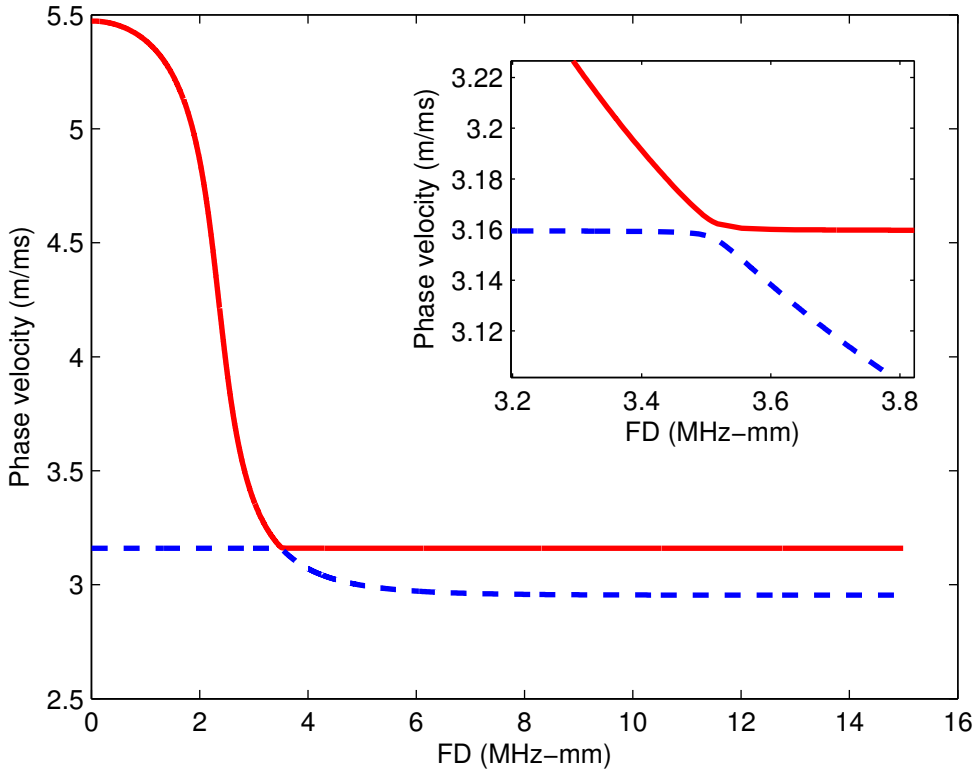

Figure 7. (color online) Dispersion curves for the S_0 and SH_0 modes for a uniaxial load of 100 MPa and propagation at an angle of 45° to the applied load. The inset plot shows that the modes are mixed and do not cross.

Approved for public release; distribution unlimited

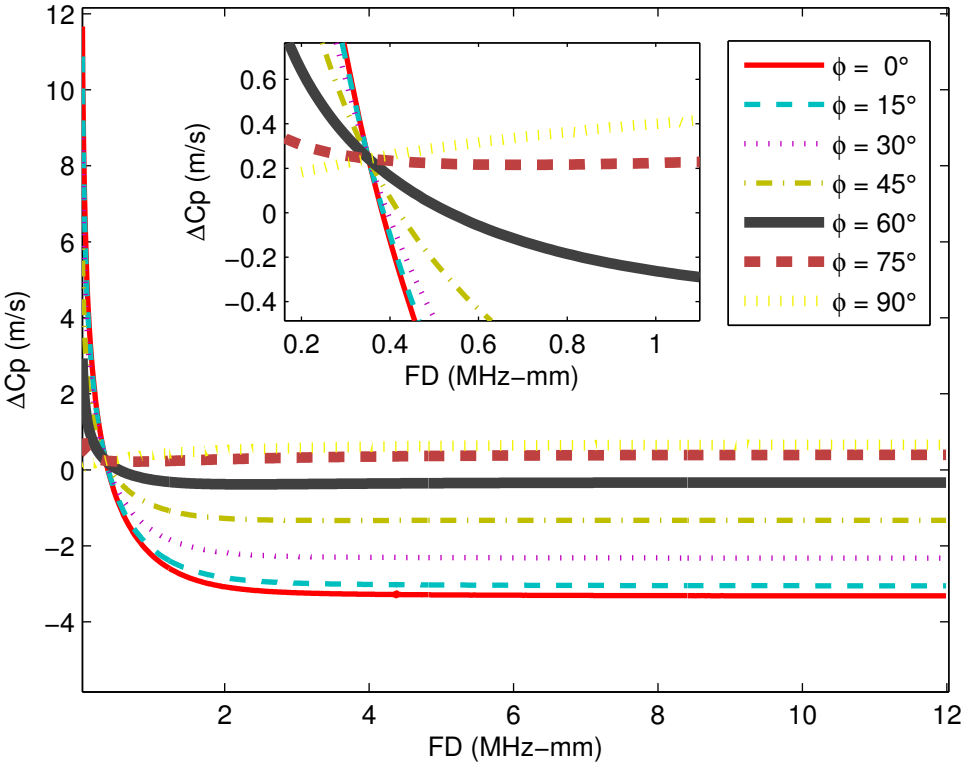

Figure 8. (color online) Changes in phase velocity for the A_0 mode propagating in steel for a uniaxial load of 100 MPa applied along the x axis (0°). The inset plot shows that the changes are isotropic for a frequency-thickness product of approximately 0.35 MHz-mm.

Approved for public release; distribution unlimited

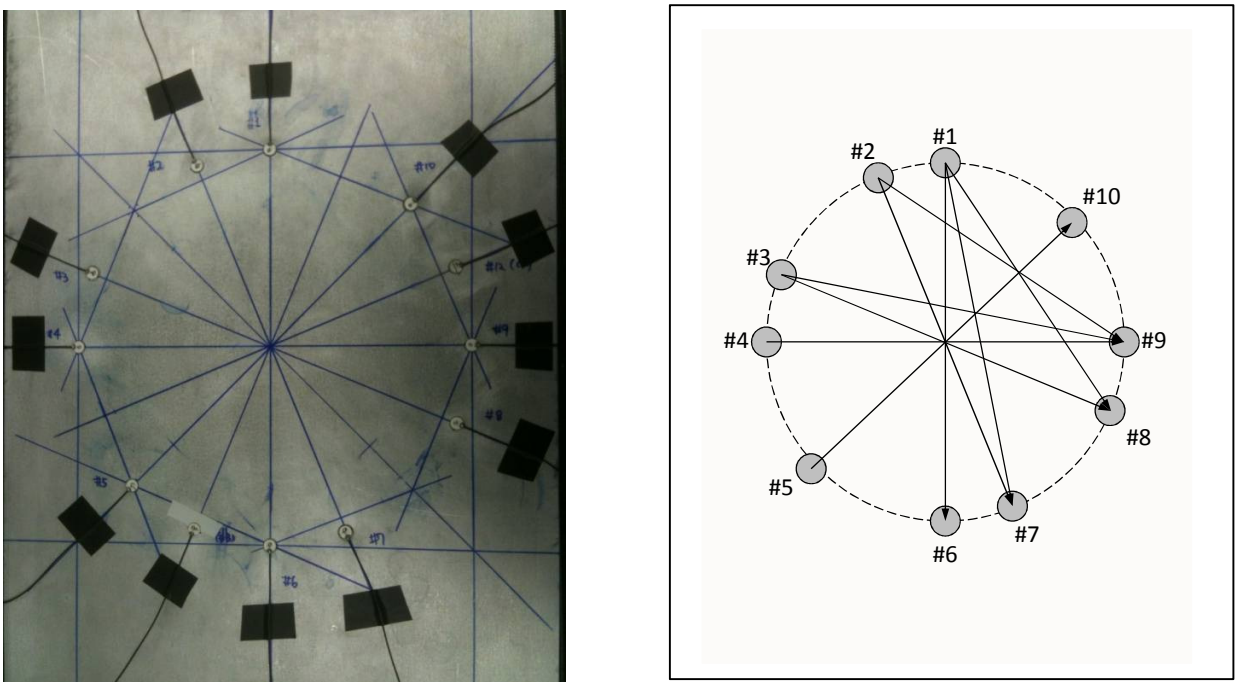

Figure 9. (a) Photograph and (b) sketch of transducers mounted to a 6.35 mm thick aluminum plate. The sketch shows the nine propagation paths used to experimentally characterize acoustoelastic Lamb wave propagation.

Approved for public release; distribution unlimited

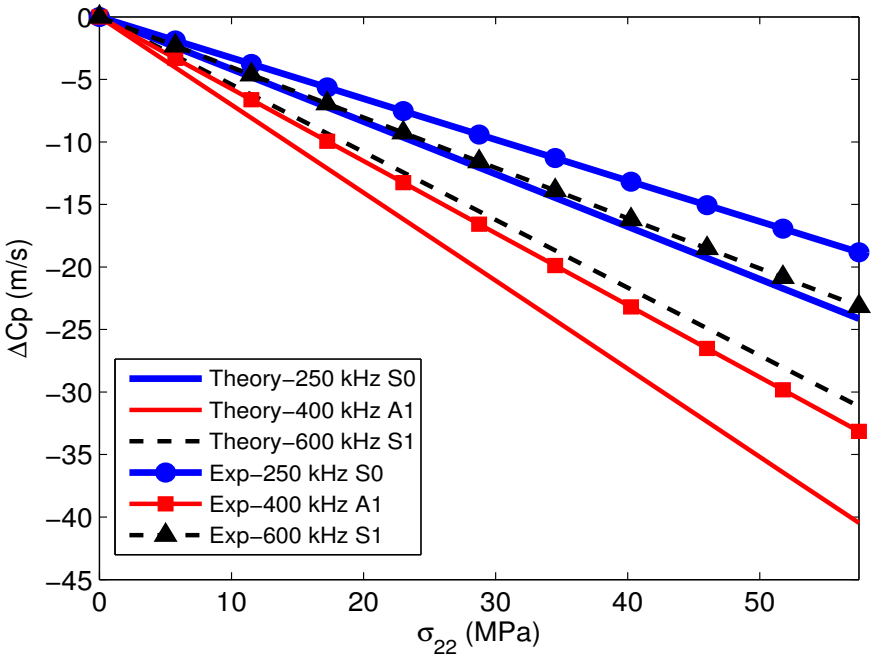

(a)

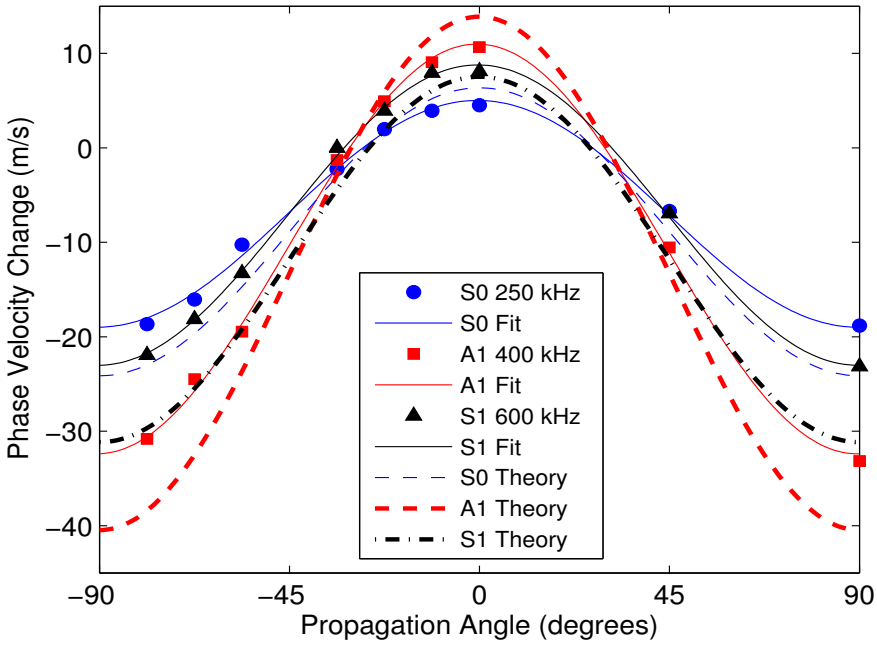

(b)

Figure 10. (color online) Comparison of theory and experiment for propagation in aluminum (thickness of 6.35 mm) with an applied uniaxial load at 90°. (a) Changes in phase velocity versus load for waves propagating at an angle of 90°, and (b) changes in phase velocity versus propagation angle for an applied load of 57.5 MPa.

Approved for public release; distribution unlimited

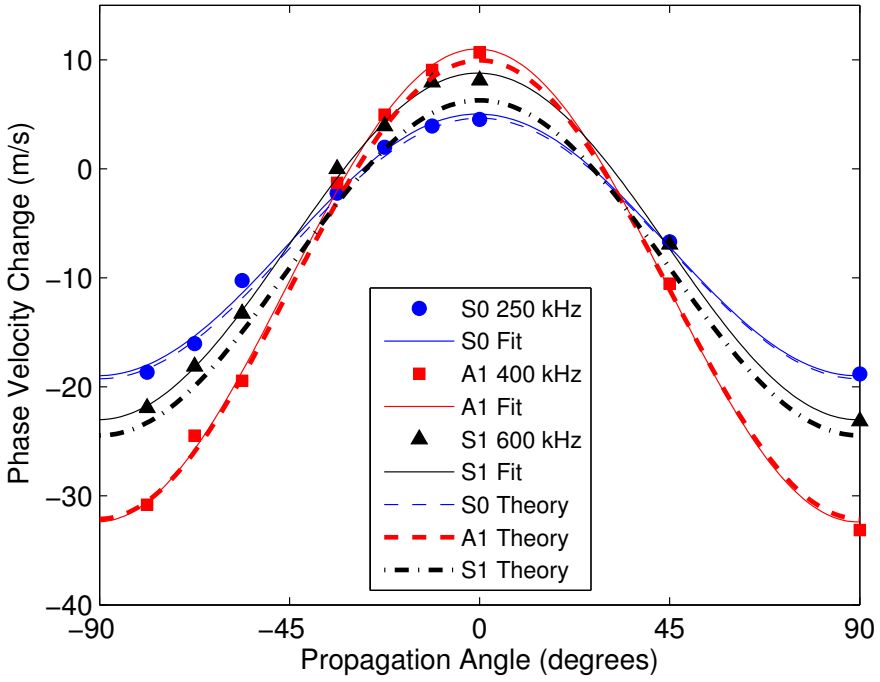

Figure 11. (color online) Comparison of theory and experiment with an applied uniaxial load of 57.5 GPa at 90° using modified TOECs (l = -181 MPa, m = -289 MPa, and n = -336 MPa).

Approved for public release; distribution unlimited